Current Applied Physics 31 (2021) 52–59

Contents lists available at ScienceDirect

Current Applied Physics

journal homepage: www.elsevier.com/locate/cap

Review

Absolute work function measurement by using photoelectron spectroscopy

Jeong Won Kim [a,b,*], Ansoon Kim [a,b,**]

[a] Korea Research Institute of Standards and Science (KRISS), 267 Gajeong-ro, Daejeon, 34113, South Korea
[b] Korea University of Science and Technology (UST), 217 Gajeong-ro, Daejeon, 34113, South Korea

ARTICLE INFO

Keywords:
Work function
Photoelectron spectroscopy
Surface electric dipole

ABSTRACT

Work function (WF) of a material is not only an intrinsic characteristic of bulk but also a surface property. The measurement and control of WF have been of great concern in many electronic and optical devices as the WF governs charge transfer and charge injection/collection efficiency at interfaces and emission characteristics of conventional charged particle emitters. Photoelectron spectroscopy (PES) has been mainly used to determine surface electronic structure and chemical composition. Despite the common use of this technique to measure WF, there has been a lack of discussion on how to use the PES and what to be considered to determine the absolute WF. The main contribution of this review lies in the discussion of the causes of errors when measuring WF, and provides a guide for reliable WF measurement. Along with the limitations of current measurement technology, we propose future directions for absolute WF measurement.

1. Introduction

Conventional work function (WF) of solid is the minimum thermodynamic work (or energy) needed to remove an electron within the solid and bring it to a vacuum outside the surface. However, this definition applies only to metals where the ionization energy and electron affinity are identical to the WF. For more general picture, the WF is measured as the difference in electrostatic potential for an electron between the Fermi level (E_F) and the maximum potential, vacuum level (E_{VAC}). The measured WF value is usually valid when the surface electrostatic potential varies smoothly near the surface [1]. As the semiconductor E_F usually lies within the band gap and its corresponding WF varies with surrounding parameter such as impurity doping. The electron energy level diagrams either on metal or semiconductor are illustrated in Fig. 1.

The WF value is not only an intrinsic property of pure material but it depends on a variety of parameters. Essentially, the WF is divided into bulk and surface contributions [2,3]. The bulk contribution is the energy difference between bound electron and vacuum level at an infinite distance. Thus, the WF of single elemental materials as well as binary compounds roughly correlates with Pauling's electronegativity [4]. In more detail, both atomic structures, corresponding to electron density in a solid, and bulk impurities determine the electron chemical potential of the bulk, the E_F. The calculation of the energy band structure of metal and the E_F position in impurity-doped semiconductor are already well established. Nevertheless, it is difficult to experimentally measure the bulk contribution in a separate way because electrons must pass through the surface rather than directly exiting the bulk. For the same reason, the bulk contribution is not important either in practical use. The surface contribution stems from electric dipole distribution at the surface of the material. Same bulk materials with varying crystal face, surface atomic rearrangement or adsorbed species lead to largely alter the electric dipole distribution, or the vacuum level near the surface. For instance, the WF of tungsten single crystal varies from 4.47 to 5.25 eV depending on (111), (100), and (110) surfaces [2]. A discussion of many different factors influencing the WF has been described in detail elsewhere [1]. The theory of WF calculation began with a simple jellium model and included periodic pseudopotential for metal surfaces by local density functional formalism [5]. The advances in ab-initio calculation utilize the Green's function technique, linear-muffin-tin-orbital method, slap-supercell approximation, and Perdew–Burke–Ernzerhof generalized gradient approximation, respectively [6–9]. Their results reach close agreement with the experimental WF values for single elements. The recent theoretical studies enable to predict the WF changes upon alloying [10], surface adsorption [11], step formation [12], and nanostructure surface formation [13].

While metals are full of electrons up to the E_F, semiconductors have a forbidden energy gap for electrons. The E_F of semiconductor lies in the gap, which causes variable WF values depending on the E_F position.

* Corresponding author. Korea Research Institute of Standards and Science (KRISS), 267 Gajeong-ro, Daejeon, 34113, South Korea.
** Corresponding author. Korea Research Institute of Standards and Science (KRISS), 267 Gajeong-ro, Daejeon, 34113, South Korea.
E-mail addresses: jeongwonk@kriss.re.kr (J.W. Kim), askim@kriss.re.kr (A. Kim).

https://doi.org/10.1016/j.cap.2021.07.018
Received 6 March 2021; Received in revised form 11 June 2021; Accepted 25 July 2021
Available online 3 August 2021

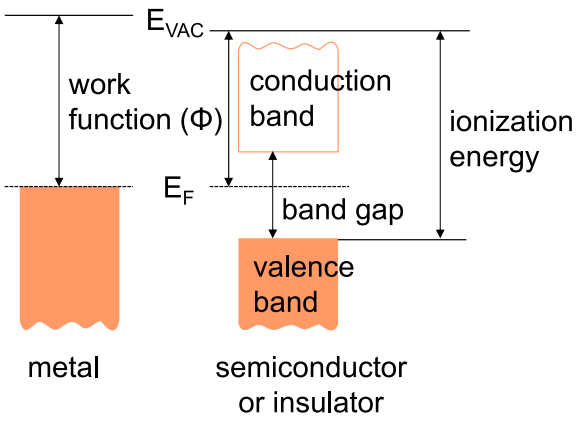

Fig. 1. Schematic energy diagram of work function (Φ) on a metal and a semiconductor.

Apart from the bulk E_F level determined by doping type and concentration, surface states created by atomic reconstruction causes the surface E_F level pinning. Depending on the surface state properties, additional dipoles occur due to charge redistribution and space charge layers. Thus, the calculation of semiconductor WF becomes more complicated [14].

People initially recognized the importance of WF in terms of the threshold energy for Einstein's photoelectric event on free surfaces and Edison's thermionic emission from a hot cathode. Since the WF directly determines the emission capabilities of conventional electron or ion emitters [15,16], researchers or engineers should consider the cathode WF when they design the emitter source. More recently, many optical and electronic devices, comprising multiple stack of different materials, show a strong dependence of interface charge injection/collection efficiency on the WF of constituent materials. Fig. 2 shows the schematic energy level diagram of a metal and a semiconductor before and after making the contact. The difference between the WF (φ_M) of metal and the electron affinity (χ_S) of semiconductor counts for the charge distribution after contact. In thermal equilibrium, the Fermi levels of metal (E_F^M) and semiconductor (E_F^S) should be aligned, resulting in charge redistribution at the interface. Therefore, the difference between φ_M and χ_S results in forming an interface dipole which greatly influences the band bending (V_B) and Schottky barrier formation (φ_{SB})at the interface [17,18]. For practical examples, indium tin oxide (ITO) is the most popular anode material for transparent electrode in display and solar cell devices. Considering the device performance, the hole injection efficiency from ITO to next semiconductor material or electron blocking layer and vice versa has been a great concern, and thus the WF control and its measurement of each material has been an importance task [19,20].

In modern metal-oxide-semiconductor field-effect transistors (MOSFETs), a proper choice of gate material and its surface treatment becomes to be important because the integration of high-k dielectric oxide layer into the metal gate needs to set the WF in gate in order to achieve a desired threshold voltage [21,22]. Furthermore, the suitable WF value in photocatalyst system has been turned out to correlate directly with its efficient photocatalysis [23–26]. As increasing the metal WF in metallized TiO_2 powder [25], higher yield of ammonia was produced due to the efficient light-induced charge separation.

In electrochemistry, the WF of electrode and its relation with electrode potential has been studied to explore the interface of electrode and electrolyte for the understanding of electrochemical reactions. The WF of electrode measured after immersion in electrolyte showed the linear correlation with the electrode potential during immersion, with a slope of 1 ± 0.1 for Au, Ag, Pt, and Ir electrodes [27–30]. The linear potential induced change in WF on the electrode is associated with the electric double layer formation at the solid-electrolyte interface. This correlation can provide a somewhat indirect way to measure the WF of clean metal electrode. Furthermore, in Li-based battery technologies, the control of the interaction of Li metal with its surroundings is critical for the availability of stable Li metal anodes. Even though in the ideal case, the anode surface should be ionically conductive but electronically insulating, the decrease of its work function caused by interaction with environmental gas would enhance the reduction of electrolyte molecules [31]. In addition to the various experiments, the importance of heterogeneous electron transfer rate constant on metal WF was studied [26], which enables to explain experimental data for different metals, solvents, supporting electrolytes, and electroactive species.

Due to the importance of material WF, accurate and reproducible measurements of the WF have been taken as a major step for material characterization in various devices. This is because the WF of individual material is an important parameter in the design of device. This review compares several different techniques used for the modern WF measurement. Among them, a special focus on photoelectron spectroscopy (PES) is provided because of its frequent use and wide application. To expand its application and improve the accuracy and reliability for measuring WF, we here describe important factors and issues to be considered upon the measurement.

2. Comparison of WF measurement techniques

The WF measurement has been carried out on the basis of several different physical phenomena such as thermionic emission, filed emis-

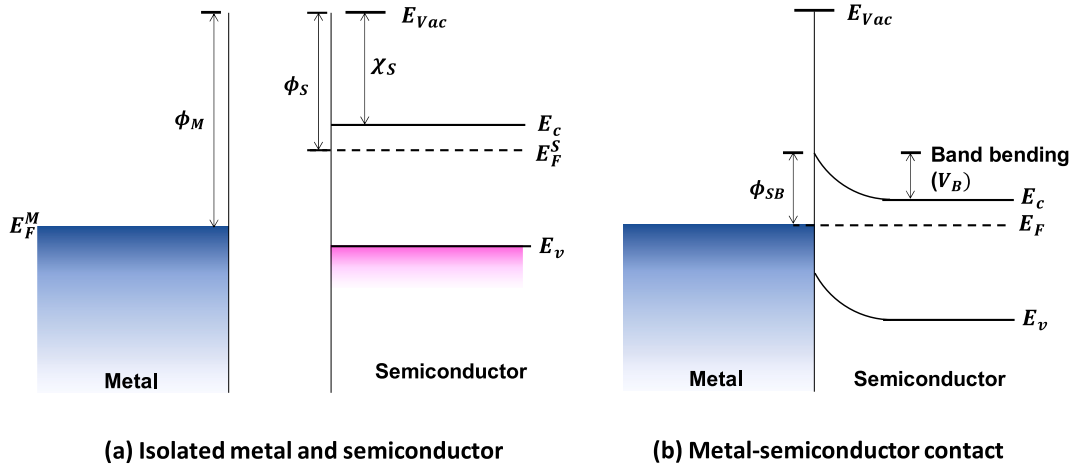

Fig. 2. Schematic energy diagram (a) before and (b) after metal-semiconductor contact.

Table 1
Comparison of work function measurement techniques.

Principle	Requirement	Advantage	Disadvantage
Thermionic emission (TE)	Stable materials at high temperatures	Rather simple	Sample with high temperature endurance
Field emission (FE)	Materials made into a fine tip	Applicable to field emission microscope depending crystal orientation	Various Effects on tip radius and microfield
Photoelectric effect (PE)	Electron spectrometer	Compatible with common UPS or XPS technique	Average WF value over a large area (0.1–3 mm)
	Tunable photon source from visible to DUV and photodetector	Applicable to any substance near ambient condition	Ionization energy (rather than WF) detected for semiconductor
Contact potential difference (CPD)	Reference electrode, usually gold	Applicable to insulator	WF significantly relies on tip condition

sion, photoelectric emission, and contact potential difference [4,32–36]. The comparison of the WF measurement techniques is listed in Table 1. The thermionic emission occurs when thermal energy enough to overcome the WF of material is provided to charge carriers in the material. The thermionic current governed by Richardson's law is exponentially proportional to the WF at low current regime [37,38]. Thus, the thermionic WF of solid controls the electronic current density, J, emitted from a conductor at temperature T. As can be deduced from the correlation, the thermionic WF equals to $-\mathrm{kTln}(J/AT^2)$, where k and A are Boltzmann's constant and Richardson's constant, respectively. The Richardson's constant, A, is given by $A = (4\pi mk^2e)/h^3 = 1.20173 \times 10^6$ $\mathrm{Am}^{-2}\mathrm{K}^{-2}$, where m and e are the mass and charge of electron, respectively, and h is Planck's constant. However, this thermionic emission method generally requires a target material that can survive at high temperatures. Field emission enables electrons to be emitted by quantum mechanical tunnelling under a high electric field. In this process, the local emission current density is described by Fowler-Nordheim equation [39]. In order to enhance the field emission, a sample should be made into a very sharp tip. A dense array of carbon nanotube bundles is a good and practical sample for the use of field emission technique [40].

Photoelectric emission occurs when the photon energy is greater than the sample WF. One of the most popular and widely used techniques for the WF measurement is based on this photoelectric emission. This technique is to measure the minimum photon energy required to liberate electrons from a substance on the basis of PE. By varying the energy of the incoming light, the photoelectric WF can be established. An ambient-pressure photoemission method using variable wavelength of light is already in commercial use [41]. On the other hand, at a constant and high enough photon energy, one can also measure kinetic energies (*KEs*) of photoelectrons by an electron analyser to estimate the WF. Using a monochromatic light source with a known wavelength, the absolute WF value can be estimated.

The next popular method is Kelvin probe (KP) technique, [42] where relative surface potential is measured by forming a capacitor between conductive probe tip and sample. This method becomes one of key techniques in the field of atomic force microscope (AFM). The scanning Kelvin probe microscope (SKPM) possesses nanometre-scale lateral resolution but its measured value always relies on tip condition and measurement environment [43]. Thus, the KP technique does not give an absolute value but a relative WF.

Among the above methods, the electron spectroscopy produces a sharp secondary electron cutoff (SEC) for the WF determination [20,44,45]. Furthermore, X-ray photoelectron spectroscopy (XPS) or ultraviolet photoelectron spectroscopy (UPS) users can easily adopt this method without any additional equipment modification or additional sampling procedure. That is because it is based on a well-developed high--resolution electron analyser with concentric hemispherical shape and a well-defined photon energy source from rare-gas discharge or monochromatized X-ray. Similar measurement principle of secondary electron emission induced by electron or ion beam [46,47] has been used. However, this method requires samples to be stable inorganic materials that are resistant to particle-induced damage. Furthermore, charged particle radiation and emission require a constant electrical potential of sample during the measurement. Otherwise, the different electric potential of sample makes the *KE* position shift or broaden the emitted electron. In that sense, an electrically insulating sample is difficult to measure its WF by electron spectroscopy. Nonetheless, the photoelectron spectroscopy is an important and practical method because the measured value is applicable directly to various solid-state electronic devices. In particular, the WF of semiconductor is difficult to be measured by other methods.

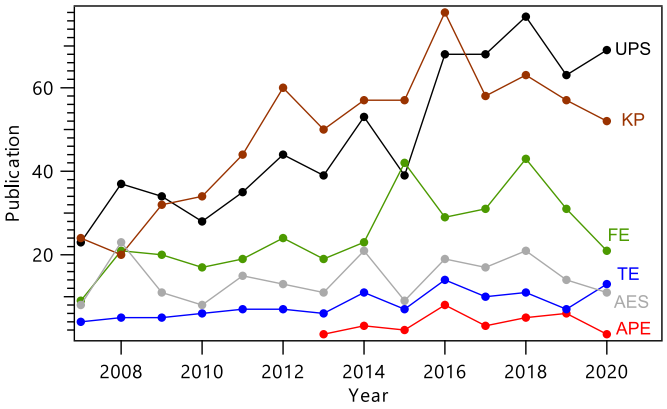

Fig. 3. The number of publications per year regarding the WF measurement by various methods @SCOPUS. UPS, KP (Kelvin probe), FE (field emission), AES (Auger electron spectroscopy), TE (thermionic emission), and APE (ambient-pressure photoemission).

Fig. 3 shows the comparison of the numbers of publications over the past decade years concerning various WF measurement techniques. Majority of WF measurements has been performed by UPS and KP. While the UPS provides an area-average WF, the KP can probe local WFs depending on the effective probe size. Thus, the sensitivity and accuracy strongly depend on specific measurement system. The recent increase of their publications is due to the modern development of electron energy analyser and scanning probe technologies. As a result, more than 65% of the well-known WF values for materials have been reported based on the photoelectric effect measurement [48,49].

3. WF measurement by UPS

According to the photoelectric effect, the photon irradiation onto a solid sample induces photoelectron emission with various *KEs*. Fig. 4 illustrates how to define the WF of metal and semiconductor from

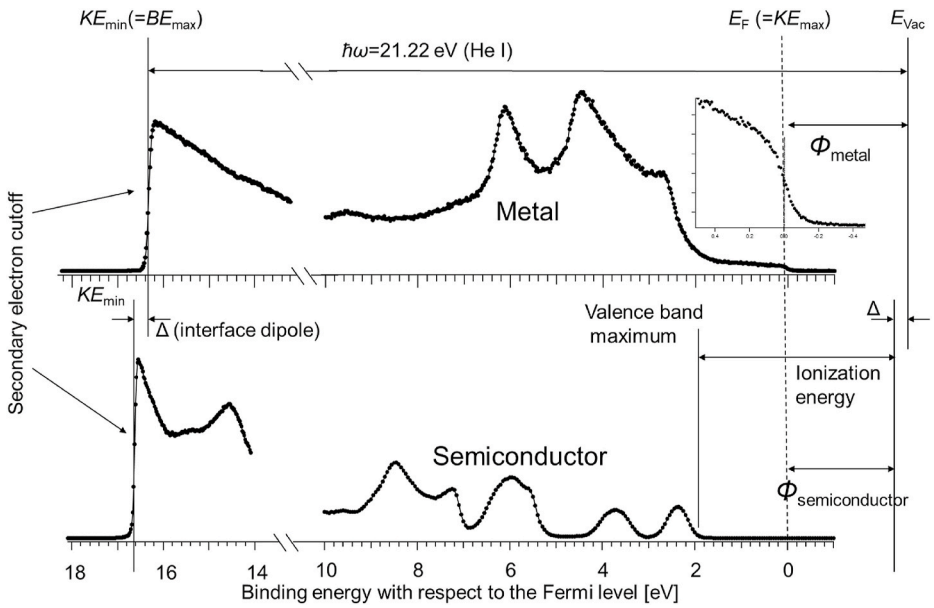

Fig. 4. Illustration of WF measurement by UPS (He I light source) for metal and semiconductor. Once the Fermi level (E_F) is established by spectrometer calibration, one only needs to measure the secondary electron cutoff (SEC) position. Here Δ means the WF difference of the two materials.

photoelectron spectrum measured by UPS (He I light source). The total photoelectron spectrum (Fig. 4) obtained from electron spectrometer is displayed in the range between photon energy ($\hbar\omega$) and sample WF. The maximum kinetic energy (KE_{max}) of photoelectrons emitted from a metal is defined as Fermi level (E_F). Since the emitted photoelectrons are collected through an electron spectrometer, the WF of spectrometer should be considered to measure sample WF. Due to the spectrometer WF, one needs to calibrate the spectrometer energy scale by determining the E_F position using a noble metal surface after surface cleaning. The inset shows an example of the Fermi edge. At a limited energy resolution, the first derivative of the spectrum can be fitted with a Gaussian function. The detailed procedures of UPS energy scale calibration and the Fermi level determination are described elsewhere [50–52].

Practically, one should measure the minimum *KE* (KE_{min}) from the SEC and the KE_{max} from the E_F to estimate the sample WF according to the following equation (1) [3,53–55].

$$\mathrm{WF} = \hbar\omega - |KE_{max} - KE_{min}| = \hbar\omega - |BE_{max} - E_F| \quad (1)$$

If the spectrometer energy scale is well calibrated, the E_F position for the KE_{max} electron can be established, in which the electron binding energy (*BE*) becomes zero. Therefore, the spectrometer WF is not necessary to be considered afterwards. What has to be measured is the position of KE_{min} or SEC position. In other words, the sample WF is calculated from the width of total spectrum $|KE_{max} - KE_{min}|$ or the maximum binding energy (BE_{max}) in equation (1). As the right side of the SEC includes the density of states of the corresponding material on top of the secondary electron background, a general simulation of the SEC shape is not possible. However, when the cutoff spectrum exhibits sigmoidal shape, the SEC can be represented by an extended logistic function [56,57]. Otherwise, one can draw three linear line fittings along the SEC.

When semiconductor and metal materials are put together in contact as a typical interface structure of electric devices, the metal WF and semiconductor ionization energy govern the energy level alignment according to Schottky-Mott rule, as long as they do not generate interface chemical reaction as in Fig. 2. However, the electrical charge redistribution upon equilibrium between the two materials could bring a change in the vacuum level and concurrent band bending of semiconductor. This charge redistribution builds up the interface dipole (Δ), as shown in Fig. 4, which plays a critical role in the prediction of carrier transfer characteristics at a heterogeneous junction [55,58].

Since the secondary electrons with low *KEs* are collected by an electron analyser for the WF measurement, the electron analyser should be able to detect the low *KE* electrons down to a few eV. To collect the reliable electron signal by a conventional hemisphere-type electrostatic analyser, at least a few eV of electron *KE* is needed in practical way. Thus, a certain amount of negative bias voltage is necessary to accelerate the photoelectron towards the spectrometer. The bias voltage can be optimized with respect to a measurement system or sample holder geometry. A low bias voltage is preferred as long as the low background and sharp SEC are observed. Otherwise the high electric field between sample and analyser input lens deteriorates emitted electron pathway. Nonetheless, the low energy electrons are so vulnerable to surrounding electric and magnetic field. For that reason, the analysis chamber should be properly shielded from remnant magnetic field. Currently, Mu-metal, which is nickel-iron alloys with very high magnetic permeability, is widely used for manufacturing chambers to screen the magnetic field. Otherwise, the SEC position is not well identified because the earth's magnetic field alters the electron trajectory. Another requirement for the WF measurement is the electron emission geometry normal to the analyser axis at the sample surface. Off-normal emission geometry may alter the symmetric distribution of the electric field between the sample surface and the analyser input lens [53]. Thus, an angle-resolved electron analyser with narrow acceptance angle is desirable. In addition, uneven structures around the sample may interfere with the electric field and should also be avoided [1].

4. Effect of surface contamination, roughness, and inhomogeneity

Since the WF is so sensitive to surface condition, even minor modification to the surface brings a dramatic change in the WF. This property has inversely been used as a measurement submonolayer thickness of species adsorbed on clean surfaces. Strong electronegative or positive adsorbates cause clear WF changes [59,60] unless they are chemically too reactive. The measured value heavily depends on surface cleanliness and homogeneity for a single metal substance. Even after cleaning the surface under ultrahigh vacuum (UHV) condition, the WF changes are often observed over time due to the contamination within the UHV chamber. Fig. 5 shows the WF changes of Au measured by UPS with time

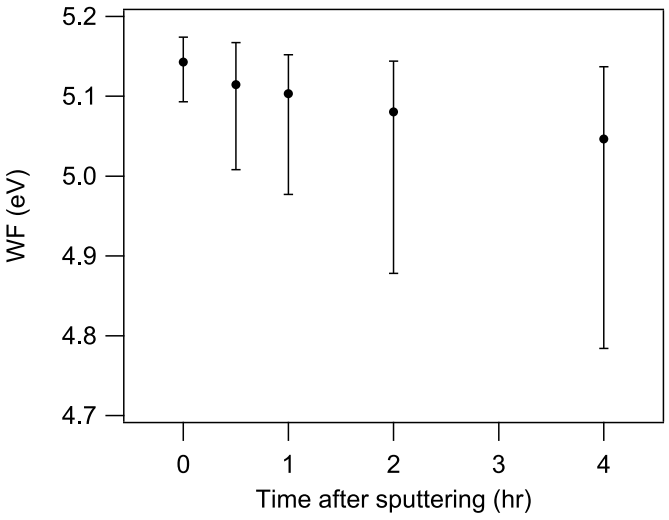

Fig. 5. Work function values of Au measured by UPS with time after Ar $^{+}$ sputter-cleaning. The base pressure of the chamber is 3×10^{-10} Torr. Error bars are their minimum and maximum values of nine different points within the 8 × 8 mm sample.

after Ar^{+} sputter-cleaning (3 kV for 30 min). The WF continues to decrease over time, even when the sample remains in UHV condition. A small amount of residual gas present in the chamber can be adsorbed on the clean Au surface, which compresses the tail of electronic dipole at the metal surface. The metal WF decrease with exposing time in UHV (Fig. 5) is a result of so-called pillow effect or cushion effect [61,62]. In addition, the measured WF values show wide scattering distribution with time. In particular, the minimum value within the error decreases more rapidly than the maximum value, which indicates the inhomogeneous contamination process over the surface. Notwithstanding, quantifying the surface contamination with XPS signal is difficult due to the % detection limit.

Another parameter that may influence the WF is surface roughness. A previous report indicates that the WF decreases with surface roughness [63]. Fig. 6 shows the WF variation of copper as increasing surface roughness proved by experiments and simulations. This result indicates that the microstructures such as grain shape and grain size of specimen surface with different surface roughness should induce the significant WF change. This model is examined only on highly rough surfaces above 30 nm of surface roughness.

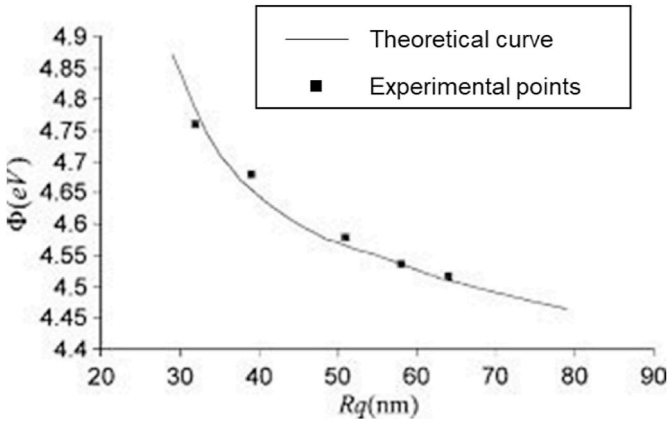

Fig. 6. Work function variation of copper with different surface roughness (R_q). Reproduced with permission from Ref. [63]. Copyright © 2005 American Institute of Physics.

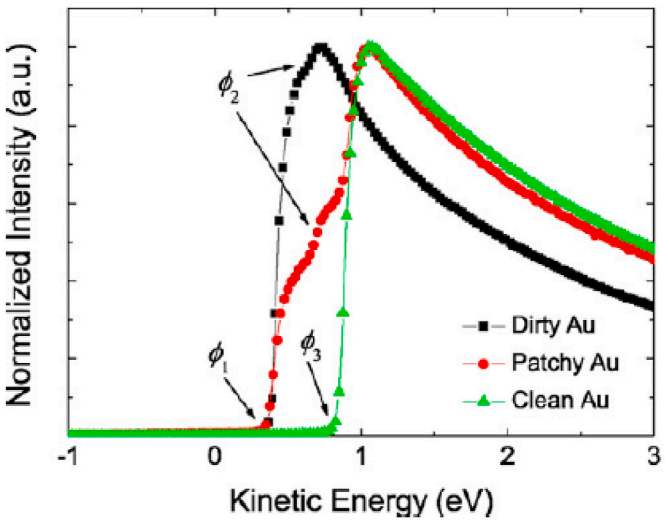

Fig. 7. SEC region of UPS spectra for inhomogeneous surface. Patchy Au surface shows three different WFs ($\phi_1 - \phi_3$), while clean and dirty sample surfaces show distinct WF values, ϕ_1 and ϕ_3, respectively. Reproduced with permission from Ref. [53]. Copyright 2010 Elsevier.

Non-uniform surface patches of a few μm size sometime generates multiple SECs and pitfalls in WF measurements [53,64]. When dirty and clean surfaces coexist, the SEC shows two different locations as shown in Fig. 7. An atomically inhomogeneous structure can be created by the steps on metal crystal surfaces. The WF decreases linearly with the step density for W(100) surface [65]. This phenomenon is interpreted as each step orientation giving a different direction of electric dipole, reducing the net dipole relative to the flat surface.

Another way to measure WF on a heterogeneous surface is the photoemission from adsorbed xenon (PAX) [66]. The UPS generally produces an ensemble average value over a few mm area and the electron charge distribution smoothens the electric potential on the surface. Thus, an atomically inhomogeneous surface will produce wide or multiple slopes in the SEC signal. As a result, the UPS cannot distinguish such different regions at all. But, the strong polarizability and chemically inert nature of Xe adsorbed on the surface results in the independent energy level alignment with E_{VAC}. Thus, the Xe 5p measurement gives the information of local WF on atomically inhomogeneous surfaces [67]. But, the PAX requires the low-temperature sample cooling below 80 K, which hampers wider applications.

5. Future directions

For the measurement of insulator samples, positively charged holes left behind the electron emission cause an electric potential shift, which limits reliable SEC measurement. Irregular charging effect on sample surface (so-called differential charging) may bring additional broad or multiple feature of the SEC. The charging problem is dependent on sample resistivity, temperature, and light intensity. Compared to UPS, XPS neutralization methods such as electron flood gun (in combination with a pulsed ion gun), sample heating, UV irradiation, etc. are relatively well established within commercial machines [68,69]. Thus, the XPS can be the better choice of WF measurement for many types of insulating samples.

Despite this advantage, the WF determination with the low-*KE* SEC and E_F in the XPS demands a wide range of scale linearity over a few thousand eV due to the use of high X-ray source energy compared to UPS. Fig. 8 illustrates the WF measurement by XPS with Al Kα light source, where the total XPS spectrum obtained from electron spectrometer is displayed in the range between photon energy ($\hbar\omega$) and sample WF. Compared with UPS measurement (Fig. 4), the total range is

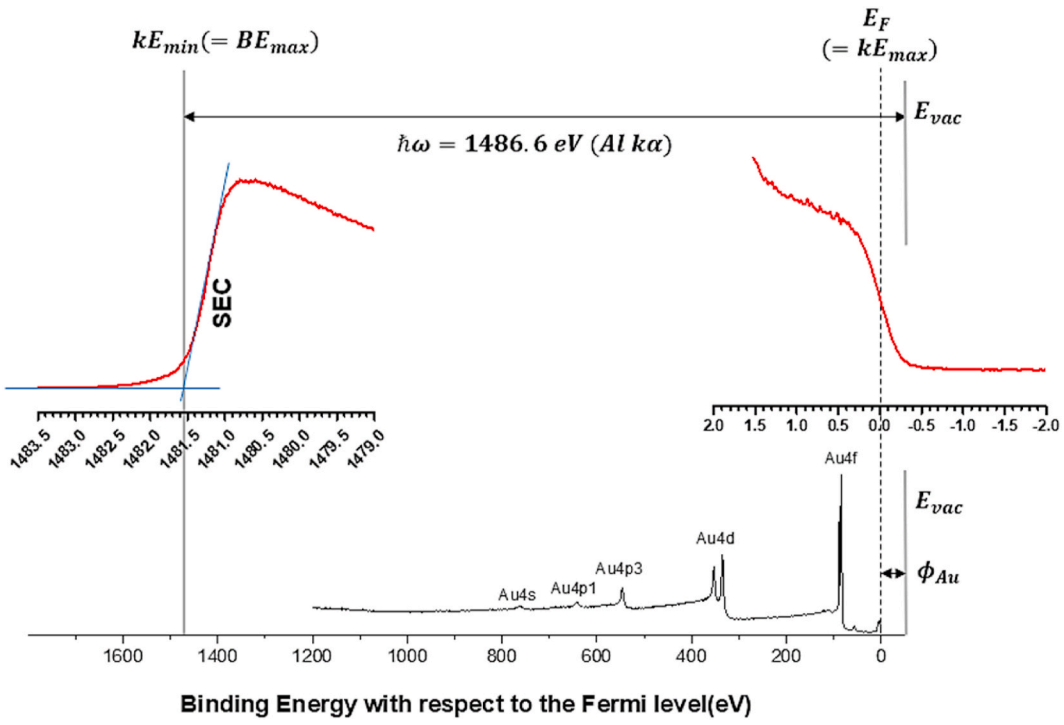

Fig. 8. Illustration of WF measurement by XPS (Al Kα light source) of clean Au.

much wider for WF measurement by XPS. Without a guarantee of the scale linearity within this wide range, using XPS measurement raises additional concern to estimate the accurate WF. Furthermore, the relatively low energy resolution of XPS causes further uncertainty in WF determination compared to UPS. Most XPS users often use it for the WF measurement without understanding these weak points [70,71]. Thus, when using XPS, the absolute WF value should be carefully determined due to the above reasons. In case of using adventitious carbon-adsorbed films as *BE* referencing method in XPS, the C 1s *BE* relative to E_F from the hydrocarbon varies over a wide range of 2 eV or more depending on the substrate, and correlates well with the underlying sample WF [72,73]. The consequence of E_{VAC} alignment between the adventitious carbon layer and the underlying sample significantly reduces the standard deviation of C 1s *BE* relative to E_{VAC} rather than to E_F. A similar concept has been applied for the absolute WF determination by using ambient pressure XPS, where Ar gas is in dynamic contact with sample surface. There is a good correlation between several known surfaces and the WF of the Ar 2p core level *BE* [74]. Thus, the above examples are good alternatives to UPS using XPS when performing WF measurement on unknown materials.

Whether a WF measurement technique gives absolute or relative value, any reference material could be useful to calibrate a photoelectron spectrometer. In particular, the KP method enables to measure the relative WF between sample and tip, where the reference material is strongly required to measure the WF of unknown material. However, the uniformity and stability of reference candidates has not been carefully examined so far. There are lots of known WF values for pure materials in literature. But, the values were obtained from clean crystal surfaces, which are not easily accessible in ordinary laboratories, because they need in-situ cleaning procedure. Furthermore, their surfaces are not stable at all in air. One of old conventional references is highly oriented pyrolytic graphite (HOPG) with the WF of 4.4–4.7 eV [75–77]. Indeed, many KP users use the HOPG as a reference due to its relatively stable surface under ambient condition. However, the HOPG grade and crystal orientation distribution influence the actual value. The use of HOPG as reference for PES-based WF measurement needs further investigation such as HOPG grade and surface cleaning method. Another type of potential WF references is self-assembled monolayer (SAM) formed onto surface. Depending on molecular structure, the WF of indium tin oxide has been controlled in a wide range [78,79]. This SAM-based surface can be a good candidate for WF reference standards. Kant et al. theoretically analyzed the influence of molecular polarity of SAM, its dipolar orientation and electrode surface morphology on average WF [80–82]. Therefore, the suitability for the SAM-based WF standards can be decided by considering these effects. Similarly, a polymer composite has successfully been used to control the WF. Depending on the ratio of two different polymer concentration, self-organized surface showed WF variation on the ITO [83]. Another candidate for the WF reference is gold film because it has an even and inert surface compared to other metals, good conductivity for PES-based WF measurement, and maintains a clean surface in UHV during WF measurement after sputtering. Nonetheless, one must be aware of the surface cleanness because a thin film of polycrystalline gold exhibits a WF of 4.4–4.7 eV when exposed to air [62]. As shown in Fig. 5, the Ar^+ sputtering in UHV reduces the WF variation (error bar) of the gold. Therefore, well-defined sputtering method under UHV can provide the gold as a WF reference.

6. Conclusion

The WF has long been a well-known physical parameter, but in recent years the importance of its absolute value control has emerged due to sophisticated modern electronic devices. The demand for WF evaluation of new materials will increase. Since the PES is a widely used technique not only in academy but also in industry, we reviewed the pros and cons of the PES for the WF measurements. Knowing the PES characteristics will help users measure the WF values that will be used more frequently in the future. To achieve reliable WF measurements, the appropriate selections of machine operation condition, measurement geometry, and sample surface are required. Extending UPS to XPS and adding proper reference materials for WF measurements will have a greater impact on material and device development.

Declaration of competing interest

The authors declare that they have no known competing financial interests or personal relationships that could have appeared to influence the work reported in this paper.

Acknowledgements

This work was supported by the National Research Foundation (NRF) (grant No. NRF-2020M3H4A3081882 and 2019M3D1A1078299).

Appendix A. Supplementary data

Supplementary data to this article can be found online at https://doi.org/10.1016/j.cap.2021.07.018.

References

[1] M. Yoshitake, Work Function and Band Alignment of Electrode Materials, Springer Japan, 2021.
[2] H. Ishii, K. Sugiyama, E. Ito, K. Seki, Energy level alignment and interfacial electronic structures at organic/metal and organic/organic interfaces, Adv. Mater. 11 (1999) 605–625.
[3] D. Cahen, A. Kahn, Electron energetics at surfaces and interfaces: concepts and experiments, Adv. Mater. 15 (2003) 271–277.
[4] J. Hölzl, F.K. Schulte, in: J. Hölzl, F.K. Schulte, H. Wagner (Eds.), In Solid Surface Physics, Springer Berlin Heidelberg, Berlin, Heidelberg, 1979, pp. 1–150.
[5] N.D. Lang, W. Kohn, Theory of metal surfaces: charge density and surface energy, Phys. Rev. B 1 (1970) 4555–4568.
[6] H.L. Skriver, N.M. Rosengaard, Surface energy and work function of elemental metals, Phys. Rev. B 46 (1992) 7157–7168.
[7] M. Methfessel, D. Hennig, M. Scheffler, Trends of the surface relaxations, surface energies, and work functions of the 4d transition metals, Phys. Rev. B 46 (1992) 4816–4829.
[8] N.E. Singh-Miller, N. Marzari, Surface energies, work functions, and surface relaxations of low-index metallic surfaces from first principles, Phys. Rev. B 80 (2009) 235407.
[9] D.-P. Ji, Q. Zhu, S.-Q. Wang, Detailed first-principles studies on surface energy and work function of hexagonal metals, Surf. Sci. 651 (2016) 137–146.
[10] J.A. Rothschild, M. Eizenberg, Work function calculation of solid solution alloys using the image force model, Phys. Rev. B 81 (2010) 224201.
[11] M.-L. Bocquet, A.M. Rappe, H.-L. Dai, A density functional theory study of adsorbate-induced work function change and binding energy: olefins on Ag(111), Mol. Phys. 103 (2005) 883–890.
[12] J. White, J. Liu, J.J. Hinsch, Y. Wang, Theoretical understanding of the properties of stepped iron surfaces with van der Waals interaction corrections, Phys. Chem. Chem. Phys. 23 (2021) 2649–2657.
[13] J. Kaur, R. Kant, Theory of work function and potential of zero charge for metal nanostructured and rough electrodes, J. Phys. Chem. C 121 (2017) 13059–13069.
[14] W. Mönch, Work Function and Band Bending at Semiconductor Surfaces, Springer, Berlin, Heidelberg, 1984.
[15] S. Yamamoto, Fundamental physics of vacuum electron sources, Rep. Prog. Phys. 69 (2006) 181–232.
[16] H. Kawano, Effective work functions for ionic and electronic emissions from mono- and polycrystalline surfaces, Prog. Surf. Sci. 83 (2008) 1–165.
[17] L.J. Brillson, Chemical reaction and charge redistribution at metal–semiconductor interfaces, J. Vac. Sci. Technol. 15 (1978) 1378–1383.
[18] H. Lüth, Solid Surfaces, Interfaces and Thin Films, sixth ed., Springer, 2015.
[19] Y. Park, V. Choong, Y. Gao, B.R. Hsieh, C.W. Tang, Work function of indium tin oxide transparent conductor measured by photoelectron spectroscopy, Appl. Phys. Lett. 68 (1996) 2699–2701.
[20] R. Schlaf, H. Murata, Z.H. Kafafi, Work function measurements on indium tin oxide films, J. Electron. Spectrosc. Relat. Phenom. 120 (2001) 149–154.
[21] E. Erben, K. Hempel, D. Triyoso, in: K.H. Yeap, H. Nisar, IntechOpen (Eds.), In Complementary-Metal-Oxide-Semiconductor, 2018.
[22] R. Lin, L. Qiang, P. Ranade, K. Tsu-Jae, H. Chenming, An adjustable work function technology using Mo gate for CMOS devices, IEEE Electron. Device Lett. 23 (2002) 49–51.
[23] C. Peng, P. Wei, X. Li, Y. Liu, Y. Cao, H. Wang, H. Yu, F. Peng, L. Zhang, B. Zhang, High efficiency photocatalytic hydrogen production over ternary Cu/TiO2@Ti3C2Tx enabled by low-work-function 2D titanium carbide, Nanomater. Energy 53 (2018) 97–107.
[24] L. Wang, J. Ge, A. Wang, M. Deng, X. Wang, S. Bai, R. Li, J. Jiang, Q. Zhang, Y. Luo, Designing p-type semiconductor–metal hybrid structures for improved photocatalysis, Angew. Chem. 126 (2014) 5207–5211.
[25] Y. Nosaka, K. Norimatsu, H. Miyama, The function of metals in metal-compounded semiconductor photocatalysts, Chem. Phys. Lett. 106 (1984) 128–131.
[26] R. Kant, J. Kaur, G.K. Mishra, Theory for influence of the metal electrolyte interface on heterogeneous electron transfer rate constant: fractional electron transferred transition state approach, J. Phys. Chem. C 124 (2020) 2273–2288.
[27] D. Rath, D. Kolb, Continuous work function monitoring for electrode emersion, Surf. Sci. 109 (1981) 641–647.
[28] E. Kötz, H. Neff, K. Müller, A. Ups, XPS and work function study of emersed silver, platinum and gold electrodes, J. Electroanal. Chem. Interfacial Electrochem. 215 (1986) 331–344.
[29] H. Neff, R. Kötz, Photoelectron spectroscopic study of emersed gold electrodes, J. Electroanal. Chem. Interfacial Electrochem. 151 (1983) 305–310.
[30] E. Kötz, H. Neff, Anodic iridium oxide films: an UPS study of emersed electrodes, Surf. Sci. 160 (1985) 517–530.
[31] A. Etxebarria, S.L. Koch, O. Bondarchuk, S. Passerini, G. Teobaldi, M.Á. Muñoz-Márquez, Work function evolution in Li anode processing, Adv. Energy Mater. 10 (2020) 2000520.
[32] M. Cardona, L. Ley, Photoemission in Solids I, Springer-Verlag, Berlin, 1978.
[33] S. Yamamoto, Fundamental physics of vacuum electron sources, Rep. Prog. Phys. 69 (2005) 181.
[34] O. Klyushnikov, Method to determine the work function using X-ray photoelectron spectroscopy, J. Struct. Chem. 39 (1998) 944–947.
[35] J. Kim, B. Lägel, E. Moons, N. Johansson, I. Baikie, W.R. Salaneck, R. Friend, F. Cacialli, Kelvin probe and ultraviolet photoemission measurements of indium tin oxide work function: a comparison, Synth. Met. 111 (2000) 311–314.
[36] R. Strayer, W. Mackie, L. Swanson, Work function measurements by the field emission retarding potential method, Surf. Sci. 34 (1973) 225–248.
[37] O.W. Richardson, The Emission of Electricity from Hot Bodies, Longmans Green and Company, London, 1921.
[38] C. Herring, M.H. Nichols, Thermionic Emission, Rev. Mod. Phys. 21 (1949) 185–270.
[39] R.H. Fowler, L. Nordheim, Electron emission in intense electric fields, Proc. R. Soc. London, Ser. A 119 (1928) 173–181.
[40] O. Gröning, O.M. Küttel, C. Emmenegger, P. Gröning, L. Schlapbach, Field emission properties of carbon nanotubes, J. Vac. Sci. Technol., B 18 (2000) 665–678.
[41] I.D. Baikie, A. Grain, J. Sutherland, J. Law, Near ambient pressure photoemission spectroscopy of metal and semiconductor surfaces, Phys. Status Solidi C 12 (2015) 259–262.
[42] M. Nonnenmacher, M.P. O'Boyle, H.K. Wickramasinghe, Kelvin probe force microscopy, Appl. Phys. Lett. 58 (1991) 2921–2923.
[43] A. Liscio, V. Palermo, K. Müllen, P. Samorì, Tip−Sample interactions in Kelvin probe force microscopy: quantitative measurement of the local surface potential, J. Phys. Chem. C 112 (2008) 17368–17377.
[44] S. Yang, A. Kim, J. Park, H. Kwon, P.T. Lanh, S. Hong, K.J. Kim, J.W. Kim, Thermal annealing of black phosphorus for etching and protection, Appl. Surf. Sci. 457 (2018) 773–779.
[45] S.M. Park, Y.H. Kim, Y. Yi, H.-Y. Oh, J.W. Kim, Insertion of an organic interlayer for hole current enhancement in inverted organic light emitting devices, Appl. Phys. Lett. 97 (2010), 063308.
[46] Y. Nakanishi, T. Nagatomi, Y. Takai, Change in work function during phase transition of Sc–O/W(100) system at high temperatures, Appl. Surf. Sci. 256 (2009) 1082–1087.
[47] T. Nagatomi, T. Kuwayama, Y. Takai, K. Yoshino, Y. Morita, M. Kitagawa, M. Nishitani, Application of ion scattering spectroscopy to measurement of surface potential of MgO thin film under ion irradiation, Appl. Phys. Lett. 92 (2008), 084104.
[48] H.B. Michaelson, The work function of the elements and its periodicity, J. Appl. Phys. 48 (1977) 4729–4733.
[49] D.R. Lide. CRC-Handbook of Chemistry and Physics, CRC Press, Boca Raton, FL, 2005.
[50] S. Hüfner, Photoelectron Spectroscopy, 3 ed., Springer-Verlag, Berlin Heidelberg, 2003.
[51] F. Patthey, J.-M. Imer, W.-D. Schneider, H. Beck, Y. Baer, High-resolution photoemission study of the low-energy excitations in 4f-electron systems, Phys. Rev. B 42 (1990) 8864–8881.
[52] J.W. Rabalais, Principles of Ultraviolet Photoelectron Spectroscopy, John Wiley & Sons, New York, 1977.
[53] M.G. Helander, M.T. Greiner, Z.B. Wang, Z.H. Lu, Pitfalls in measuring work function using photoelectron spectroscopy, Appl. Surf. Sci. 256 (2010) 2602–2605.
[54] S. Braun, W.R. Salaneck, M. Fahlman, Energy-level alignment at organic/metal and organic/organic interfaces, Adv. Mater. 21 (2009) 1450–1472.
[55] Y. Gao, Surface analytical studies of interfaces in organic semiconductor devices, Mater. Sci. Eng. R Rep. 68 (2010) 39–87.
[56] W.H. Kirchhoff, Logistic function profile fit: a least-squares program for fitting interface profiles to an extended logistic function, J. Vac. Sci. Technol.: Vacuum, Surfaces, and Films 30 (2012), 051101.
[57] S.A. Wight, C.J. Powell, Evaluation of the shapes of Auger-and secondary-electron line scans across interfaces with the logistic function, J. Vac. Sci. Technol.: Vacuum, Surfaces, and Films 24 (2006) 1024–1030.
[58] A. Kahn, N. Koch, W. Gao, Electronic structure and electrical properties of interfaces between metals and π-conjugated molecular films, J. Polym. Sci., Part B: Polym. Phys. 41 (2003) 2529–2548.
[59] J.W. Kim, J.M. Seo, S. Kim, Surface electronic properties of Na/Ge(111)-3x1, Surf. Sci. 351 (1996) L239–L244.
[60] T. Roman, A. Groß, Periodic density-functional calculations on work-function change induced by adsorption of halogens on Cu(111), Phys. Rev. Lett. 110 (2013) 156804.
[61] H. Vázquez, Y.J. Dappe, J. Ortega, F. Flores, Energy level alignment at metal/organic semiconductor interfaces: "Pillow" effect, induced density of interface states, and charge neutrality level, J. Chem. Phys. 126 (2007) 144703.

[62] A. Kahn, Fermi level, work function and vacuum level, Mater. Horiz. 3 (2016) 7–10.
[63] W. Li, D.Y. Li, On the correlation between surface roughness and work function in copper, J. Chem. Phys. 122 (2005), 064708.
[64] T. Schultz, P. Amsalem, N.B. Kotadiya, T. Lenz, P.W.M. Blom, N. Koch, Importance of substrate work function homogeneity for reliable ionization energy determination by photoelectron spectroscopy, Phys. Status Solidi B 256 (2018) 1800299.
[65] B. Krahl-Urban, E.A. Niekisch, H. Wagner, Work function of stepped tungsten single crystal surfaces, Surf. Sci. 64 (1977) 52–68.
[66] K. Wandelt, The local work function: concept and implications, Appl. Surf. Sci. 111 (1997) 1–10.
[67] A.J. Gellman, L. Baker, B.S. Holsclaw, Xe adsorption site distributions on Pt(111), Pt(221) and Pt(531), Surf. Sci. 646 (2016) 83–89.
[68] Surface chemical analysis — X-ray photoelectron spectroscopy — Reporting of methods used for charge control and charge correction, ISO 19318:2004.
[69] D.R. Baer, K. Artyushkova, H. Cohen, C.D. Easton, M. Engelhard, T.R. Gengenbach, G. Greczynski, P. Mack, D.J. Morgan, A. Roberts, XPS guide: charge neutralization and binding energy referencing for insulating samples, J. Vac. Sci. Technol. 38 (2020), 031204.
[70] S. Evans, Work function measurements by X-Pe spectroscopy, and their relevance to the calibration of X-Pe spectra, Chem. Phys. Lett. 23 (1973) 134–138.
[71] J.Q. Wu, Y. Zhang, B. Wang, F.T. Yi, S.Z. Deng, N.S. Xu, J. Chen, Effects of X-ray irradiation on the structure and field electron emission properties of vertically aligned few-layer graphene, Nucl. Instrum. Methods Phys. Res. Sect. B Beam Interact. Mater. Atoms 304 (2013) 49–56.
[72] G. Greczynski, L. Hultman, Reliable determination of chemical state in x-ray photoelectron spectroscopy based on sample-work-function referencing to adventitious carbon: resolving the myth of apparent constant binding energy of the C 1s peak, Appl. Surf. Sci. 451 (2018) 99–103.
[73] G. Greczynski, L. Hultman, X-ray photoelectron spectroscopy: towards reliable binding energy referencing, Prog. Mater. Sci. 107 (2020) 100591.
[74] S. Axnanda, M. Scheele, E. Crumlin, B. Mao, R. Chang, S. Rani, M. Faiz, S. Wang, A. P. Alivisatos, Z. Liu, Direct work function measurement by gas phase photoelectron spectroscopy and its application on PbS nanoparticles, Nano Lett. 13 (2013) 6176–6182.
[75] D. Wrana, K. Cieślik, W. Belza, C. Rodenbücher, K. Szot, F. Krok, Kelvin probe force microscopy work function characterization of transition metal oxide crystals under ongoing reduction and oxidation, Beilstein J. Nanotechnol. 10 (2019) 1596–1607.
[76] W.N. Hansen, G.J. Hansen, Standard reference surfaces for work function measurements in air, Surf. Sci. 481 (2001) 172–184.
[77] P.A.F. Garrillo, B. Grévin, N. Chevalier, Ł. Borowik, Calibrated work function mapping by Kelvin probe force microscopy, Rev. Sci. Instrum. 89 (2018), 043702.
[78] A. Sharma, B. Kippelen, P.J. Hotchkiss, S.R. Marder, Stabilization of the work function of indium tin oxide using organic surface modifiers in organic light-emitting diodes, Appl. Phys. Lett. 93 (2008) 163308.
[79] F.S. Benneckendorf, S. Hillebrandt, F. Ullrich, V. Rohnacher, S. Hietzschold, D. Jänsch, J. Freudenberg, S. Beck, E. Mankel, W. Jaegermann, A. Pucci, U.H. F. Bunz, K. Müllen, Structure–property relationship of phenylene-based self-assembled monolayers for record low work function of indium tin oxide, J. Phys. Chem. Lett. 9 (2018) 3731–3737.
[80] M.B. Singh, R. Kant, Shape-and size-dependent electronic capacitance in nanostructured materials, Proc. Math. Phys. Eng. Sci. 469 (2013) 20130163.
[81] J. Kaur, R. Kant, Curvature-induced anomalous enhancement in the work function of nanostructures, J. Phys. Chem. Lett. 6 (2015) 2870–2874.
[82] J. Kaur, R. Kant, Model of local work function and PZC for molecular self assembly over nanostructured metal electrode, J. Phys. Chem. C 122 (2018) 911–918.
[83] K.-G. Lim, H.-B. Kim, J. Jeong, H. Kim, J.Y. Kim, T.-W. Lee, Boosting the power conversion efficiency of perovskite solar cells using self-organized polymeric hole extraction layers with high work function, Adv. Mater. 26 (2014) 6461–6466.